JOURNAL OF GUIDANCE, CONTROL, AND DYNAMICS
Vol. 40, No. 4, April 2017

Fast Computable Recoverable Sets and Their Use for Aircraft Loss-of-Control Handling

Kevin McDonough* and Ilya Kolmanovsky†
University of Michigan, Ann Arbor, Michigan 48109

DOI: 10.2514/1.G001747

The paper describes a framework for constrained flight control based on the use of recoverable sets that are chained together to guide constrained admissible transitions between trim points. The recoverable set is the set of all states for which there exists a control sequence such that the subsequent response is guaranteed to satisfy the imposed constraints. The constraints can reflect actuator range/rate limits, safety limits, as well as ranges of validity of the aircraft model. Because in aircraft loss-of-control situations, fast onboard computations are necessary, the approach to computing recoverable sets in this paper exploits linear discrete-time models (which can be generated via onboard system identification and reflect effects of failures and degradations) and recovery sequences generated, either by a stable linear finite-dimensional subsystem or through a reset of the dynamic controller states or of its set points. With this approach, only subsets of the full recoverable set can be computed, however, these recoverable subsets possess certain desirable control invariance properties, and their computations are simple; moreover, the onboard generation of the recovery sequence reduces to a low-dimensional quadratic programming problem. The applications of this approach to longitudinal and lateral linearized and nonlinear aircraft flight models are reported.

Nomenclature

b	=	wing span
c	=	mean wing chord
O_∞	=	safe set
p	=	roll rate
q	=	pitch rate
R_∞	=	recoverable set
r	=	yaw rate
S	=	wing surface area
U_0	=	nominal air speed
U, V, W	=	X, Y, Z components of aircraft airspeed
α	=	angle of attack
β	=	sideslip angle
γ	=	flight-path angle
Δx	=	perturbed state in linearized system model
$\delta_a, \delta_e, \delta_r$	=	aileron, elevator, and rudder angles
δ_T	=	thrust
θ	=	pitch angle
ρ	=	air density
ϕ	=	bank angle

I. Introduction

AN AIRCRAFT loss-of-control (LOC) event is defined by Wilborn and Foster [1], based on a large study of aviation accidents jointly performed by NASA and The Boeing Company [2], as an excursion from three or more critical envelopes: the adverse aerodynamics envelope, unusual attitude envelope, structural integrity envelope, dynamic pitch control envelope, and dynamic roll envelope. These envelopes are essentially a collection of structural, control, and dynamic constraints. Although deviation from one or more of these envelopes does not immediately spell disaster for an aircraft, if more of these constraints are violated, the aircraft recovery becomes increasingly more difficult.

Techniques to characterize aircraft states that can lead to future constraint adherence or violation are thus necessary to be able to detect, prevent, and mitigate LOC events. In this paper, we focus on safe and recoverable sets as primary tools for this characterization. A safe set is the set of aircraft initial states for which the nominal closed-loop response does not violate the imposed constraints. A recoverable set is the set of aircraft initial states for which there exists control inputs as functions of time that prevent constraint violation. The literature on computing these and closely related forward and backward reachable sets for constrained aircraft dynamics is extensive (see, e.g., [3–11] and references therein). Many of the existing approaches exploit nonlinear models and require extensive computations to solve partial differential equations. Consequently, their onboard use with aircraft models being identified online in LOC situations may be infeasible unless significant simplifications are made and short horizons are assumed (see [6]).

To enable the computations of safe and recoverable sets to be feasible for onboard implementation, in this paper we focus on exploiting discrete-time linear models. In addition, we restrict the recovery mechanisms to permit simple computations of sets of recoverable states. Specifically, we consider recovery control sequences generated either by a stable linear finite-dimensional subsystem or recovery mechanisms that operate through a reset of states of the controller or through modifications of the controller set points. With this approach, only subsets of the full recoverable set are determined, however, the computations are simple and reduce to constructions of the conventional safe sets for appropriately augmented or extended systems. These recoverable subsets also possess certain desirable control invariance properties. Moreover, the onboard generation of the recovery sequence is feasible and reduces to a low-dimensional quadratic programming problem.

Finally, we demonstrate that these recoverable subsets can be exploited for constrained flight control based on chaining them together to guide constrained admissible transitions between trim points. Previous approaches based on the use of safe constraint-admissible and contractive sets [12–15] are thus generalized to the use of recoverable subsets of various kinds. These recoverable subsets can be significantly larger and enable less conservative transitions between trim points further apart to take place while employing suitable recovery sequences. Another attractive feature of our transition planning framework, as shown in [13], is being able to easily handle unmeasured additive set-bounded disturbances and uncertainties.

Presented as Paper 2014-0786 at the AIAA Guidance, Navigation, and Control Conference, National Harbor, MD, 13–17 January 2014; received 1 October 2015; accepted for publication 7 July 2016; published online 29 September 2016.

*Graduate Student Researcher, Department of Aerospace Engineering.
†Professor, Department of Aerospace Engineering.

The rest of the paper is organized as follows. In Sec. II, we describe our approach to defining and computing recoverable sets based on different recovery mechanisms, and we characterize their properties. The use of recoverable sets for constrained trim-point-to-trim-point transition planning is described in Sec. III. In Sec. IV, we describe the aircraft model and constraints. Numerical examples of recoverable sets are reported in Sec. V, in which we also illustrate their use for constrained maneuver planning and LOC prevention. Simulations based on the nonlinear aircraft model are included to validate our use of linearized models, combined with appropriate model validity constraints. Section VI presents concluding remarks.

Our previous publications [16–18] reported some of the developments described in this paper in a conference format. This paper contains generalizations, more comprehensive examples, and the results of evaluation on the nonlinear model.

II. Recoverable Sets

We consider procedures for constructing sets of initial conditions for which closed-loop trajectories of a discrete-time linear system

$$\begin{aligned} x(k+1) &= Ax(k) + Bu_c(k), \\ y(k) &= Cx(k) + Du_c(k) \end{aligned} \tag{1}$$

in which $k \in Z^+$, $x(k) \in \mathbb{R}^{n_x}$ is the state vector, $u_c(k) \in \mathbb{R}^{n_u}$ is the control vector, and $y(k) \in \mathbb{R}^{n_y}$ is the constrained output vector, can be made to satisfy constraints with an appropriate choice of control input. The constraints are given by

$$y(k) \in Y = \{y\colon Gy \le g\} \tag{2}$$

in which $G \in \mathbb{R}^{n_h \times n_y}$, $g \in \mathbb{R}^{n_h}$, and n_h is the number of inequalities that make up the output constraint set.

Note that Eq. (1) can represent a discrete-time model of open-loop linearized aircraft dynamics. The output constraints (2), in that case, are generated from consideration of the flight envelope, control constraints, and assumptions made for the region of validity of the linearized model.

A. Safe States for Closed-Loop Systems with a Static Controller

Suppose a static state feedback controller is used for the system (1) so that

$$u_c(k) = -Kx(k) \tag{3}$$

Then, the closed-loop dynamics are given by

$$\begin{aligned} x(k+1) &= A_{\mathrm{CL}}x(k), \\ y(k) &= C_{\mathrm{CL}}x(k) \end{aligned} \tag{4}$$

in which $A_{\mathrm{CL}} = A - BK$, $C_{\mathrm{CL}} = C - DK$, and the controller gain K is assumed to be stabilizing.

The response of Eq. (4) to an initial state $x(0)$ is easily predicted as

$$\begin{aligned} x(k) &= A_{\mathrm{CL}}^k x(0), \\ y(k) &= C_{\mathrm{CL}}A_{\mathrm{CL}}^k x(0) \end{aligned} \tag{5}$$

The trajectory resulting from an initial condition $x(0)$ satisfies the constraints at time k if

$$GC_{\mathrm{CL}}A_{\mathrm{CL}}^k x(0) \le g \tag{6}$$

The set of all initial conditions $x(0)$ that lead to responses that satisfy constraints for all future time instants is referred to as O_∞ [19,20]:

$$O_\infty = \{x(0) \in \mathbb{R}^{n_x}\colon y(k) = C_{\mathrm{CL}}A_{\mathrm{CL}}^k x(0) \in Y, \qquad \forall\, k \ge 0\} \tag{7}$$

If A_{CL} is Schur (i.e., the gain K is stabilizing), $(C_{\mathrm{CL}}, A_{\mathrm{CL}})$ is observable, $0 \in \mathrm{int}Y$, and Y is compact, then O_∞ is positively invariant, is finitely determined, and is a polytope (bounded polyhedron) [19]. Finite determination means that there exists t^* such that $O_\infty = O_t$ for all $t \ge t^*$, where

$$O_t = \{x(0) \in \mathbb{R}^{n_x}\colon y(k) = C_{\mathrm{CL}}A_{\mathrm{CL}}^k x(0) \in Y, \ \text{ for } k = 0, \ldots, t\} \tag{8}$$

In practice, t^* is comparable to the settling time of the closed-loop system and an upper bound on t^* can be easily estimated based on contractivity properties of the closed-loop system. The representation for O_∞ is obtained by stacking the inequality constraints

$$\begin{bmatrix} G \\ GC_{\mathrm{CL}}A_{\mathrm{CL}} \\ GC_{\mathrm{CL}}A_{\mathrm{CL}}^2 \\ \vdots \\ GC_{\mathrm{CL}}A_{\mathrm{CL}}^{t*} \end{bmatrix} x(0) \le \begin{bmatrix} g \\ g \\ \vdots \\ g \end{bmatrix} \tag{9}$$

Assuming an efficient method of performing matrix operations is being used, the inequalities (9) can be formed very quickly. Note also that some of the constraints forming O_∞ in inequality (9) may be redundant and can be eliminated to reduce storage memory requirements and simplify subsequent computations involving O_∞. Simpler subsets that closely approximate O_∞ can be generated by eliminating the almost redundant constraints and applying a pull-in transformation [21]. However, constraint elimination, often performed by linear programming, may require nonnegligible computing effort and hence may be avoided altogether in online applications. Note also that O_∞ is dependent on the choice of the nominal controller (3) and sampling period used to obtain the discrete-time model (1).

B. Recoverable States with Controller State Reset

In situations when dynamic controllers are used, the set of plant states that result in constraint-admissible responses can be enlarged through the controller state reset. In fact, controllers frequently employ integral action to guarantee offset-free tracking of constant reference commands and asymptotic rejection of constant input disturbances. For a controller with integral action, the closed-loop system is described by the following equations:

$$\begin{aligned} x(k+1) &= Ax(k) + Bu_c(k), \\ x_I(k+1) &= C_I x(k) + x_I(k) \end{aligned} \tag{10}$$

in which $x(k) \in \mathbb{R}^{n_x}$, $x_I(k) \in \mathbb{R}^{n_I}$, and

$$u_c(k) = -K_1 x(k) - K_2 x_I(k) \tag{11}$$

The closed-loop system model can be written as

$$\begin{aligned} \bar{x}(k+1) &= \bar{A}\,\bar{x}(k), \\ \bar{y}(k) &= \bar{C}\,\bar{x}(k) \end{aligned} \tag{12}$$

in which

$$\bar{x}(k) = \begin{bmatrix} x(k) \\ x_I(k) \end{bmatrix} \tag{13}$$

$$\bar{A} = \begin{bmatrix} A - BK_1 & -BK_2 \\ C_I & I \end{bmatrix} \tag{14}$$

and $\bar{y} \in \mathbb{R}^{n_{\bar{y}}}$, $\bar{C}$ are appropriately defined to reflect the constrained outputs. The constraints have the form

$$\bar{y}(k) \in \bar{Y} = \{\bar{y}\colon \bar{G}\,\bar{y} \le \bar{g}\} \tag{15}$$

The safe set for this closed-loop system is defined as the set of all initial plant and controller states $\bar{x}(0)$, such that the ensuing closed-loop trajectories are constraint admissible. We denote this set by

$$O_\infty^I = \{\bar{x}(0) \in \mathbb{R}^{n_x+n_I}\colon \bar{C}\bar{A}^k\bar{x}(0) \in \bar{Y}, \forall\ k \ge 0\} \tag{16}$$

If $\bar{A}$ is Schur, $(\bar{C}, \bar{A})$ is observable, $0 \in \text{int}\bar{Y}$, and $\bar{Y}$ is compact, O_∞^I in Eq. (16) is positively invariant, is finitely determined, and is a polytope [19]. Similar to inequality (9), the inequality representation for O_∞^I in can be generated through constraint stacking as

$$\begin{bmatrix} \bar{G} \\ \bar{G}\bar{C}\bar{A} \\ \bar{G}\bar{C}\bar{A}^2 \\ \vdots \\ \bar{G}\bar{C}\bar{A}^{t*} \end{bmatrix} \bar{x}(0) \le \begin{bmatrix} \bar{g} \\ \bar{g} \\ \vdots \\ \bar{g} \end{bmatrix} \tag{17}$$

Note that, unlike the plant state, the controller state x_I can be reset if this facilitates the constraint enforcement. The set of plant states that can be recovered (i.e., the ensuing closed-loop response can be made to satisfy constraints) by resetting the controller state is a projection of O_∞^I onto the plant states, that is,

$$R_\infty^I = \{x(0)\colon \exists x_I(0) \text{ such that } (x(0), x_I(0)) \in O_\infty^I\} \tag{18}$$

We note that R_∞^I possesses a desirable control invariance property that can be exploited in the construction of constrained control schemes. Specifically, $x(k) \in R_\infty^I$ and $x_I(k)$ being selected consistently with the requirement that $(x(k), x_I(k)) \in O_\infty^I$, imply that $x(k+1) \in R_\infty^I$.

Finding a suitable $x_I(0)$ for a given $x(0) \in R_\infty^I$ can be posed as a quadratic programming problem similar to the one used in the controller state governor (CSG) [17,18,22]. Specifically, the reset of the controller states aims at the decrease of the closed-loop energy, as defined by a Lyapunov function

$$V_L(\bar{x}(k)) = \bar{x}(k)^T P_L \bar{x}(k) \tag{19}$$

in which $P_L = P_L^T > 0$ is the positive-definite symmetric matrix satisfying the following Lyapunov equation:

$$\bar{A}^T P_L \bar{A} - P_L + Q_L = 0 \tag{20}$$

in which $Q_L = Q_L^T > 0$. Then, the state $x_I(0)$ is determined based on the solution of the following quadratic programming problem:

$$\begin{aligned} x_I^*(0) &= \arg\min_{x_I(0)} V_L(\bar{x}(0)) \\ \text{subject to} \quad \bar{x}(0) &= [x(0)^T, x_I(0)^T]^T \in O_\infty^I \end{aligned} \tag{21}$$

The CSG [17] actually exploits this strategy at every time instant k, not just at $k = 0$, to produce a constraint-admissible response that also has faster convergence through the repeated minimization of the closed-loop system energy. We note that, although in this paper we explicitly consider dynamic controllers based on integral action (11), other dynamic controllers can be treated analogously.

C. Recoverable States Through Controller State Reset and Adjustable Reference

Tracking controllers respond to reference commands and lead to closed-loop systems of the form

$$\begin{aligned} \bar{x}(k+1) &= \bar{A}\,\bar{x}(k) + \bar{B}r(k), \\ \bar{y}(k) &= \bar{C}\,\bar{x}(k) + \bar{D}r(k) \end{aligned} \tag{22}$$

in which $r(k) \in \mathbb{R}^{n_r}$ is the reference command, $\bar{B} \in \mathbb{R}^{(n+n_I)\times n_r}$, $\bar{C} \in \mathbb{R}^{n_{\bar{y}}\times(n+n_I)}$, and $\bar{D} \in \mathbb{R}^{n_{\bar{y}}\times n_r}$. The state $\bar{x}(k)$ is of the form of Eq. (13) and is composed of resettable controller states x_I and nonresettable plant states x. For instance, Eq. (22) may result from replacing the integrator dynamics in Eq. (10) by

$$x_I(k+1) = x_I(k) + C_I x(k) - r(k) \tag{23}$$

The matrix $\bar{A}$ is assumed to be Schur. Let $\bar{x}_e = H_r r$, $H_r = (I - \bar{A})^{-1}\bar{B}$, denote the equilibrium state corresponding to a constant command $r(k) \equiv r$.

The safe set for Eq. (22) is defined as the set of all initial closed-loop states $\bar{x}(0)$ and constant reference commands r, such that the ensuing closed-loop response satisfies the following constraints:

$$\begin{aligned} O_\infty^{I,r} = \{&(\bar{x}(0), r)\colon \bar{y}(k) = \bar{C}(I - \bar{A}^k)(I - \bar{A})^{-1}\bar{B}r + \bar{A}^k\bar{x}(0) \\ &+ \bar{D}r \in Y, (\bar{C}H_r + \bar{D})r \in (1-\epsilon)Y\} \end{aligned} \tag{24}$$

The last constraint

$$(\bar{C}H_r + \bar{D})r \in (1-\epsilon)Y \tag{25}$$

in which $\epsilon > 0$ is sufficiently small, tightens constraints on r in steady state to guarantee finite determination [21] of $O_\infty^{I,r}$. By stacking inequalities, we obtain a representation for $O_\infty^{I,r}$ in the form

$$\begin{bmatrix} [\bar{G}\,\bar{C}\ \ \bar{G}\,\bar{D}] \\ [\bar{G}\,\bar{C}\,\bar{A}\ \ \bar{G}\,\bar{C}(I-\bar{A})(I-\bar{A})^{-1}\bar{B} + \bar{G}\,\bar{D}] \\ [\bar{G}\,\bar{C}\,\bar{A}^2\ \ \bar{G}\,\bar{C}(I-\bar{A}^2)(I-\bar{A})^{-1}\bar{B} + \bar{G}\,\bar{D}] \\ \vdots \\ [\bar{G}\,\bar{C}\,\bar{A}^{t*}\ \ \bar{G}\,\bar{C}(I-\bar{A}^{t*})(I-\bar{A})^{-1}\bar{B} + \bar{G}\,\bar{D}] \end{bmatrix} \begin{bmatrix} \bar{x}(0) \\ r \end{bmatrix} \le \begin{bmatrix} \bar{g} \\ \bar{g} \\ \vdots \\ \bar{g} \end{bmatrix} \tag{26}$$

The set of plant states that can be recovered is the projection of $O_\infty^{I,r}$ onto the plant states

$$R_\infty^{I,r} = \left\{x(0)\colon \exists (x_I(0), r) \text{ such that } ((x(0), x_I(0)), r) \in O_\infty^{I,r}\right\} \tag{27}$$

We note that $R_\infty^{I,r}$ possesses a desirable control invariance property that can be exploited in the construction of constrained control schemes. Specifically, $x(k) \in R_\infty^{I,r}$ and $x_I(k)$, $r(k)$ being selected consistently with $((x(k), x_I(k)), r(k)) \in O_\infty^I$, imply that $x(k+1) \in R_\infty^{I,r}$.

Finding a suitable $x_I(0)$ and r for a given $x(0) \in R_\infty^{I,r}$ can be posed as a quadratic programming problem similar to the one exploited by the controller state and reference governor (CSRG) [17]. Specifically, the following cost function is introduced:

$$J(\bar{x}(k), r(k)) = \|\bar{x}(k) - \bar{x}_e(k)\|_{P_L}^2 + \|r(k) - \bar{r}(k)\|_\Gamma^2 \tag{28}$$

in which, for a matrix M, $\|z\|_M^2 = z^T M z$, $\bar{r}(k)$ is the desired reference at time instant k (which, e.g., could be zero if the linearization is at the desired trim point), $\Gamma = \Gamma^T > 0$ and $P_L = P_L^T > 0$ satisfies the Lyapunov equation (20) with $Q_L = Q_L^T > 0$, and the following quadratic programming problem is solved:

$$\begin{aligned} (\bar{x}^*(k), r^*(k)) &= \arg\min_{x_I(k), r(k)} J(\bar{x}(k), r(k)) \\ \text{subject to} \quad (\bar{x}(k), r(k)) &\in O_\infty^{I,r}, \bar{x}(k) = [x(k)^T, x_I(k)^T]^T \end{aligned} \tag{29}$$

The CSRG [17] actually exploits this strategy at every time instant k, not just at $k = 0$, to produce a constraint-admissible response that also has faster convergence through the repeated minimization of Eq. (29).

We note that, due to the additional flexibility gained by being able to change the reference command, $R_\infty^I \subset R_\infty^{I,r}$.

D. Recoverable States with Parametrized Feedforward Sequences

Another approach to enlarge the set of recoverable plant states is to consider simply parameterized feedforward control sequences. The

simple parameterization is achieved by generating these feedforward sequences with a stable auxiliary subsystem with a resettable subsystem state. Unlike the previous approaches, we do not rely on reset of given controller states but reset states of an auxiliary subsystem.

Consider the controller (3) augmented with a feedforward signal $v_c(k)$,

$$u_c(k) = -Kx(k) + v_c(k) \tag{30}$$

With Eq. (30), the closed-loop system takes the form

$$\begin{aligned} x(k+1) &= A_{\mathrm{CL}}x(k) + Bv_c(k), \\ y(k) &= C_{\mathrm{CL}}x(k) + Dv_c(k) \end{aligned} \tag{31}$$

in which $v_c(k)$ is the feedforward signal used to enforce the constraints (i.e., recover the plant states) as necessary.

We note that the viability set V_∞ [23,24] for Eq. (31) with constraints (2), that is, the set of all initial conditions $x(0)$, for which there exists a sequence $v(\cdot)$ that enforces the constraint, is difficult to compute. To develop a more easily computable inner approximation to V_∞, we assume that the recovery sequence is generated by an auxiliary system of the form

$$\begin{aligned} v_c(k) &= \hat{c} + \hat{C}\,\hat{x}(k), \\ \hat{x}(k+1) &= \hat{A}\,\hat{x}(k) \end{aligned} \tag{32}$$

in which $\hat{A}$ is a Schur matrix and $\hat{x}$ is the $n_{\hat{x}}$ vector state of the auxiliary system. The safe set for Eqs. (31) and (32) with constraints (2) is the set of initial plant states $x(0)$ and initial auxiliary states $\hat{x}(0)$, $\hat{c}$, such that the ensuing closed-loop trajectory is constraint admissible, that is,

$$\begin{aligned} O_\infty^{\mathrm{ext}} = \Big\{ &(x(0), \hat{c}, \hat{x}(0)) \in \mathbb{R}^{n_x+n_u+n_{\hat{x}}}\colon y(k) \in Y, \\ &k = 0, \ldots, t^*, C_{\mathrm{CL}}H_r\hat{c} + D\hat{c} \in (1-\epsilon)Y \Big\} \end{aligned} \tag{33}$$

in which $H_r = (I - A_{\mathrm{CL}})^{-1}B$. The last constraint $C_{\mathrm{CL}}H_r\hat{c} + D\hat{c} \in (1-\epsilon)Y$, in which $\epsilon > 0$ is sufficiently small, is introduced to guarantee that O_∞^{ext} is finitely determined [20].

The recoverable set is the projection of O_∞^{ext} onto the plant states:

$$R_\infty^{\mathrm{ext}} = \{x(0)\colon \exists \hat{c}, \hat{x}(0) \text{ such that } (x(0), \hat{c}, \hat{x}(0)) \in O_\infty^{\mathrm{ext}}\} \tag{34}$$

Note that, because the constraints (2) are affine, both O_∞^{ext} and R_∞^{ext} are polyhedral. From the computational standpoint, generating O_∞^{ext} and R_∞^{ext} can be accomplished using the conventional safe set computations and projection methods.

Given $x(0) \in R_\infty^{\mathrm{ext}}$, computing an appropriate $\hat{c} = \hat{c}(0)$ and $\hat{x}(0)$ for which constraints are enforced can be performed by solving a quadratic programming problem of the form

$$\begin{aligned} &\frac{1}{2}\hat{c}(0)^T\hat{c}(0) + \frac{1}{2}\hat{x}(0)^T P_r \hat{x}(0) \to \min_{\hat{c}(0),\hat{x}(0)} \\ &\quad \text{subject to} \quad (x(0), \hat{c}(0), \hat{x}(0)) \in O_\infty^{\mathrm{ext}} \end{aligned} \tag{35}$$

in which $P_r = P_r^T > 0$. The minimization in Eq. (35) aims at preserving the operation with the nominal controller and avoiding the unnecessary use of recovery sequence. Once $\hat{x}(0)$ and $\hat{c}$ are determined, the execution of Eq. (32) yields a recovery sequence for a given $x(0)$.

We note that the set R_∞^{ext} possesses a desirable control invariance property that can be exploited in the construction of constrained control schemes. Specifically, $x(k) \in R_\infty^{\mathrm{ext}}$ and $\hat{x}(k)$, $\hat{c}$ being selected consistently with $(x(k), \hat{c}(k), \hat{x}(k)) \in O_\infty^{\mathrm{ext}}$, so that $v(k) = \hat{c} + \hat{C}\,\hat{x}(k)$, implies that $x(k+1) \in R_\infty^{\mathrm{ext}}$. We also note that, for $x(0) \in O_\infty$, in which O_∞ is defined by Eq. (7), the solution of Eq. (35) yields $\hat{c}(0) = 0$ and $\hat{x}(0) = 0$.

Several choices exist for the selection of the auxiliary dynamics (32), including the shift register and Laguerre's sequence generators. These choices are motivated by related developments in the extended command governor case [25] and in the model-predictive control [26]. When using the shift register, the recovery sequence becomes equal to $\hat{c}$ after $H+1$ steps, and $\hat{A}$ and $\hat{C}$ have the form

$$\hat{A} = \begin{bmatrix} \bar{S}_1 & 0 & \cdots & 0 \\ 0 & \bar{S}_2 & \cdots & 0 \\ \vdots & \vdots & \ddots & \vdots \\ 0 & 0 & \cdots & \bar{S}_{n_u} \end{bmatrix}, \qquad \hat{C} = \begin{bmatrix} \bar{T}_1 & 0 & \cdots & 0 \\ 0 & \bar{T}_2 & \cdots & 0 \\ \vdots & \vdots & \ddots & \vdots \\ 0 & 0 & \cdots & \bar{T}_{n_u} \end{bmatrix} \tag{36}$$

with

$$\begin{aligned} \bar{S}_i &= \begin{bmatrix} 0 & 1 & 0 & \cdots & 0 \\ 0 & 0 & 1 & \cdots & 0 \\ \vdots & \vdots & \vdots & \ddots & \vdots \\ 0 & 0 & \cdots & \cdots & 1 \\ 0 & 0 & \cdots & \cdots & 0 \end{bmatrix} \in \mathbb{R}^{(H+1)\times(H+1)}, \\ \bar{T}_i &= [\,1 \quad 0 \quad \cdots \quad \cdots \quad 0\,] \in \mathbb{R}^{1\times(H+1)} \end{aligned} \tag{37}$$

with the number of blocks in $\hat{A}$ and $\hat{C}$ being equal to the number of control channels being used in the recovery sequence.

When using Laguerre's sequence generators, $\hat{A}$ and $\hat{C}$ have the form of Eq. (36) and $\bar{S}_i$ and $\bar{T}_i$ have the following structure:

$$\begin{aligned} \bar{S}_i &= \begin{bmatrix} \alpha_L & \beta_L & -\alpha_L\beta_L & \alpha_L^2\beta_L & \cdots \\ 0 & \alpha_L & \beta_L & -\alpha_L\beta_L & \cdots \\ 0 & 0 & \alpha_L & \beta_L & \cdots \\ 0 & 0 & 0 & \alpha_L & \cdots \\ \vdots & \vdots & \vdots & \vdots & \vdots \end{bmatrix}, \\ \bar{T}_i &= \sqrt{\beta_L}[\,1 \quad -\alpha_L \quad \alpha_L^2 \quad -\alpha_L^3 \quad \cdots\,] \end{aligned} \tag{38}$$

in which $\beta_L = 1 - \alpha_L^2$ and $0 \le \alpha_L \le 1$ are parameters. The choice $\alpha_L = 0$ corresponds to the shift register. Numerical examples suggest that low-dimensional Laguerre's sequence generators for $\alpha_L \neq 0$ are capable of producing a rich set of recovery sequences.

To incorporate the auxiliary subsystem dynamics with the nominal closed-loop system dynamics, we note that

$$u_c(k) = -Kx(k) + v_c(k) = -Kx(k) + \hat{c} + \hat{C}\,\hat{x}(k)$$

and thus,

$$u_c(k) = \begin{bmatrix} -K & I & \hat{C} \end{bmatrix} \begin{bmatrix} x(k) \\ \hat{c} \\ \hat{x}(k) \end{bmatrix} \tag{39}$$

Therefore, when one constructs O_∞^{ext} with the inclusion of a nominal controller using conventional safe set computation tools, the state vector becomes

$$\begin{bmatrix} x(k) \\ \hat{c} \\ \hat{x}(k) \end{bmatrix}$$

and the system dynamics and output matrices take the form

$$A_{\mathrm{ext}} = \begin{bmatrix} A - BK & B & B\hat{C} \\ 0 & I & 0 \\ 0 & 0 & \hat{A} \end{bmatrix}, \quad C_{\mathrm{ext}} = \begin{bmatrix} C & D & D\hat{C} \\ -K & I & \hat{C} \end{bmatrix} \tag{40}$$

The second row of C_{ext} is introduced to handle the constraints imposed on the control.

The expression for O_∞^{ext}, with the knowledge of t^*, has the following form:

$$\begin{bmatrix} G_{\text{ext}} \\ G_{\text{ext}}C_{\text{ext}}A_{\text{ext}} \\ G_{\text{ext}}C_{\text{ext}}A_{\text{ext}}^2 \\ \vdots \\ G_{\text{ext}}C_{\text{ext}}A_{\text{ext}}^{t^*} \end{bmatrix} \begin{bmatrix} x(0) \\ \hat{c} \\ \hat{x}(0) \end{bmatrix} \leq \begin{bmatrix} g \\ g \\ \vdots \\ g \end{bmatrix} \tag{41}$$

in which $G_{\text{ext}} = [G \quad 0 \quad 0]$. It should be noted that nothing in general can be said about the relationship of R_∞^{ext} to R_∞^I or $R_\infty^{I,r}$.

E. Recoverable States Through Resettable Controller States and Parametrized Feedforward Sequences

Various generalizations of the preceding recovery sequence generation schemes can be proposed. For instance, we can combine the reset of dynamic controller states with the use of recovery sequences generated by an auxiliary subsystem. Specifically, the dynamic controller

$$u_c(k) = -K_1 x(k) - K_2 x_I(k) + v_c(k) \tag{42}$$

can be used in place of Eq. (11) with $v_c(k)$ generated by an auxiliary subsystem (32). For this case, the safe and recoverable sets $O_\infty^{\text{ext},I}$ and $R_\infty^{\text{ext},I}$, respectively, are similarly defined. For $x(0) \in R_\infty^{\text{ext},I}$, $\hat{c} = \hat{c}(0)$, $x_I(0)$, and $\hat{x}(0)$ are determined through the solution of the following quadratic programming problem, which is a combination of Eq. (21), to reduce closed-loop system energy, and Eq. (35), to select the recovery sequence:

$$\frac{1}{2}\hat{c}(0)^T\hat{c}(0) + \frac{1}{2}\hat{x}(0)^T P_r \hat{x}(0) + \bar{x}(0)^T P_L \bar{x}(0) \rightarrow \min_{x_I(0),\hat{c}(0),\hat{x}(0)}$$
$$\text{subject to } (x(0), x_I(0), \hat{c}(0), \hat{x}(0)) \in O_\infty^{\text{ext},I} \tag{43}$$

in which P_L and P_r are defined as before.

III. Constrained Control of Trim-Point-to-Trim-Point Transitions Using Recoverable Sets

Constrained control schemes that plan and execute constraint-admissible transitions between trim points based on the use of safe/contractive sets and graph search have been proposed in our previous work [13]. Here, we describe necessary modifications to accommodate the recoverable sets.

Suppose a nonlinear model of the system has the following form:

$$X(t+1) = F(X(t), U_c(t)) \tag{44}$$

in which $X(t)$ is the vector state and $U_c(t)$ is the vector control. A point X_{eq} is a trim point of Eq. (44), if there exists a constant value of the input $U_c = U_{\text{eq}}$ for which X_{eq} is an equilibrium [i.e., $F(X_{\text{eq}}, U_{\text{eq}}) = 0$]. Two trim points are connected, if there exists a trajectory from one trim point to any open neighborhood of another trim point that does not violate constraints.

Assuming that the linearized models remain sufficiently accurate, which can be facilitated through the imposition of artificial model validity constraints, we determine the connectedness of a trim point X_{eq}^- to another trim point X_{eq}^+, based on the recoverable sets corresponding to the linearized system at X_{eq}^+. Depending on the type of safe or recoverable sets being used, one of the following conditions can be exploited:

$$X_{\text{eq}}^- - X_{\text{eq}}^+ \in O_\infty^+ \tag{45}$$

or

$$X_{\text{eq}}^- - X_{\text{eq}}^+ \in R_\infty^{I+} \tag{46}$$

or

$$X_{\text{eq}}^- - X_{\text{eq}}^+ \in R_\infty^{I,r+} \tag{47}$$

or

$$X_{\text{eq}}^- - X_{\text{eq}}^+ \in R_\infty^{\text{ext}+} \tag{48}$$

or

$$X_{\text{eq}}^- - X_{\text{eq}}^+ \in R_\infty^{\text{ext},I+} \tag{49}$$

in which the superscript "+" stands for the next trim point in the sequence.

Without loss of generality, we now consider in more detail the control logic based on recoverable sets R_∞^{ext} introduced in Sec. II.D. Other cases are treated similarly.

Suppose a connected sequence of trim points

$$\{X_{\text{eq}}^i, i = 1, \ldots, n_s\}$$

has been determined using the graph search and the corresponding recoverable sets are $R_\infty^{\text{ext},i}$ with $0 \in \text{int}R_\infty^{\text{ext},i}$. Typically, X_{eq}^1 is the initial trim point and $X_{\text{eq}}^{n_s}$ is the final trim point.

Let $X(t)$ be the current state, and suppose the previously commanded trim point is $X_{\text{eq}}^{i(t-1)}$, in which $i(t) \leq n_s$. If a feasible solution to Eq. (35) [i.e., $\hat{x}(0)$ and $\hat{c}(0)$] exist for $x(0) = X(t) - X_{\text{eq}}^{i(t-1)+1}$, that is,

$$X(t) - X_{\text{eq}}^{i(t-1)+1} \in R_\infty^{\text{ext},i(t-1)+1} \tag{50}$$

then we set $i(t) = i(t-1) + 1$ and reconfigure the controller for the next trim point in the sequence so that

$$U_c(t+k) = U_{\text{eq}}^{i(t)} - K^{i(t)}(X(t+k) - X_{\text{eq}}^{i(t)}) + v_c(t+k) \tag{51}$$

in which $U_{\text{eq}}^{i(t)}$ is the constant feedforward control necessary to maintain the equilibrium, K^i is the nominal feedback gain in Eq. (30) at the trim point i, and $v_c(t+k) = \hat{c}(0) + \hat{C}\hat{A}^k\hat{x}(0)$. This controller is applied as long as the transition condition (50) is not satisfied for the next equilibrium in the sequence or $i(t) = n_s$.

We now make several remarks on applicability of this approach in LOC situations.

Remark 1: We note that, in LOC situations (e.g., caused by wing icing or control surface malfunction), aircraft dynamics and constraints may change and hence the model, nominal controller, trim states, constraints, and recoverable sets need to be reidentified and reconfigured onboard. The dynamic model changes at the current trim point can be identified from the measured data and also used, based on flight-condition-dependent aircraft model parameterization (see the Appendix), to infer how the model and constraints may be changed at other trim points [27]. Recoverable sets calculated for the identified model and constraints at the current trim point can be scaled, exploiting a flight-condition-dependent scaling, to estimate a subset of a safe or recoverable set at a different (and not yet flown) trim point [16,22]. If model parameters and constraints have changed, the trim point transition plan can be reconfigured.

Remark 2: The actuator degradations/faults can be handled by modifying the control constraints or considering the additive set-bounded disturbance inputs. The specific approach to be taken depends on the actuator degradation type (e.g., stuck in position, stuck in a range, or controllable in a range).

Remark 3: The safe sets are dependent on the nominal controller being used in the closed loop. The recoverable sets with parameterized feedforward sequences, especially for large $n_{\hat{x}}$, are expected to provide a more controller-independent assessment of aircraft maneuvering capability. In particular, such an assessment and trim point transition plan can be used in combination with a direct adaptive controller [28]. Our procedure for assessing and planning feasible transitions can also be extended to use multiple controller gains [13].

IV. Linearized Aircraft Model, Nominal Controller Design, and Constraints

We use a standard aircraft dynamics model with parameters corresponding to the Twin Otter aircraft [29,30]. This nonlinear aircraft model is linearized about different trim conditions. Note that the longitudinal and lateral linearized dynamics are decoupled (see the Appendix).

A. Longitudinal Aircraft Dynamics Model

The state vector for the longitudinal linearized aircraft dynamics model is of the form

$$x_{\text{Long.}} = [\Delta u, \Delta\alpha, \Delta q, \Delta\theta]^T$$

and the control inputs are the elevator position and the thrust

$$u_{\text{long.}} = [\Delta\delta_e, \Delta\delta_T]^T$$

The "Δ" notation is used to designate state deviations from the corresponding equilibrium [i.e., $x(k) = \Delta X(k) = X(k) - X_{\text{eq}}$].

As an example, at the trim point corresponding to airspeed of $U_0 = 60$ m/s, altitude of 2500 m, flight-path angle of $\gamma_0 = 0$ deg, and bank angle $\phi_0 = 0$ deg, the dynamics and input matrices of the longitudinal linearized continuous-time model are

$$A_{\text{Long.}} = \begin{bmatrix} -0.0395 & 5.3887 & 0.2245 & -9.7845 \\ -0.0069 & -1.6732 & 0.9475 & 0 \\ 0 & -11.3863 & -4.1119 & 0 \\ 0 & 0 & 1 & 0 \end{bmatrix}, \quad B_{\text{Long.}} = \begin{bmatrix} 0.4977 & 0.0002 \\ -0.1163 & 0 \\ -8.4728 & 0 \\ 0 & 0 \end{bmatrix} \tag{52}$$

B. Nominal Controller Design for Longitudinal Dynamics

The nominal controller for the longitudinal dynamics is designed using Linear Quadratic plus Integral (LQ-I) control techniques. The sampling period is chosen as 0.1 s. The elevator is controlled by the discrete-time feedback law

$$\delta_e(k) = -K_{\delta_e} \begin{bmatrix} \Delta u(k) \\ \Delta\alpha(k) \\ \Delta q(k) \\ \Delta\theta(k) \\ x_{I,\gamma}(k) \end{bmatrix} \tag{53}$$

in which $x_{I,\gamma}(k)$ is the integrator of error in flight-path angle $\gamma = \theta - \alpha$. For the aforementioned trim condition, the calculated LQ-I control gain has the form

$$K_{\delta_e} = [5.036 \quad -10.288 \quad -0.353 \quad 4.083 \quad 2.453] \tag{54}$$

For the thrust, the discrete-time LQ-I controller has the following form:

$$\delta_T(k) = -K_{\delta_T} \begin{bmatrix} \Delta u(k) \\ \Delta\alpha(k) \\ \Delta q(k) \\ \Delta\theta(k) \\ x_{I,\gamma}(k) \\ x_{I,U}(k) \end{bmatrix} \tag{55}$$

in which $x_{I,U}(k)$ is the integrator of the airspeed error, and

$$K_{\delta_T} = [950.452 \quad -5279.233 \quad 229.799 \quad 5361.131 \quad 942.276 \quad -9.903] \tag{56}$$

C. Lateral Aircraft Dynamics Model

The state vector for the linearized model of aircraft lateral dynamics has the form

$$x_{\text{lat}} = [\Delta\beta, \Delta p, \Delta r, \Delta\phi]^T$$

The control inputs are the aileron and the rudder so that the control input vector is of the form

$$u_{\text{lat}} = [\Delta\delta_a, \Delta\delta_r]^T$$

For the aforementioned trim condition, the dynamics and input matrices of the lateral linearized continuous-time model are

$$A_{\text{lat}} = \begin{bmatrix} 0.2406 & 0.0044 & -1.0824 & 0.1633 \\ -6.5985 & -4.1142 & 1.7850 & 0 \\ 2.7041 & -0.3416 & -2.2539 & 0 \\ 0 & 1 & 0 & 0 \end{bmatrix}, \quad B_{\text{lat}} = \begin{bmatrix} 0.0150 & -0.0568 \\ -12.3586 & 6.8408 \\ 0.4242 & -2.6649 \\ 0 & 0 \end{bmatrix} \tag{57}$$

D. Nominal Controller Design for Lateral Dynamics

The sampling period for the lateral dynamics is 0.1 s and is the same as for the longitudinal case. The aileron controller uses the following discrete-time LQ-I feedback-law:

$$\delta_a(k) = -K_{\delta_a} \begin{bmatrix} \Delta\beta(k) \\ \Delta p(k) \\ \Delta r(k) \\ \Delta\phi(k) \\ x_{I,\phi}(k) \end{bmatrix} \tag{58}$$

in which $x_{I,\phi}(k)$ is the integrator of the error in the bank angle ϕ. For the aforementioned trim condition, the calculated LQ-I control gains for the aileron are

$$K_{\delta_a} = [0.521 \quad -1.258 \quad -0.233 \quad -9.414 \quad -2.003] \tag{59}$$

The rudder controller uses the following discrete-time LQ-I feedback law:

$$\delta_r(k) = -K_{\delta_r} \begin{bmatrix} \Delta\beta(k) \\ \Delta p(k) \\ \Delta r(k) \\ \Delta\phi(k) \\ x_{I,\phi}(k) \end{bmatrix} \tag{60}$$

in which the control gain is

$$K_{\delta_r} = [-0.013 \quad -0.067 \quad -0.001 \quad 0.521 \quad 0.114] \tag{61}$$

E. State and Control Constraints

The constraints are imposed to maintain actuators within their limits, ensure that aircraft operates within the linear model validity range, and preserve safety. The control constraints are imposed on the

four control inputs: the elevator, thrust, aileron, and rudder. In our numerical examples, these constraints have the form

$$\begin{aligned} -0.2793 \le \Delta\delta_e + \delta_{e0} \le 0.3491, \\ -0.2793 \le \Delta\delta_a + \delta_{a0} \le 0.4800, \\ -0.3491 \le \Delta\delta_r + \delta_{r0} \le 0.3491, \\ 100 \le \Delta\delta_T + \delta_{T0} \le 28{,}000 \end{aligned} \tag{62}$$

in which $\Delta\delta_e$, $\Delta\delta_a$, $\Delta\delta_r$, and $\Delta\delta_T$ are the deviations in the elevator deflection, aileron deflection, rudder deflection, and thrust, respectively, from the equilibrium values of δ_{e0}, δ_{a0}, δ_{r0}, and δ_{T0}. In the preceding, the elevator, aileron, and rudder deflections are in radians and the thrust is in newtons. Also, these constraints are imposed for the nonlinear aircraft model, which means that, once a trim condition is selected (and thus, a selection of δ_{e0}, δ_{a0}, δ_{r0}, and δ_{T0} is made), the constraints for the linearized system can be obtained. For the preceding trim condition and linearized model, $\delta_{a0} = \delta_{r0} = 0$ rad, $\delta_{e0} = -0.0644$ rad, and $\delta_{T0} = 4521$ N.

The model validity constraints are imposed on the deviation in airspeed Δu, deviation in sideslip angle $\Delta\beta$, and deviations in the body-fixed angular rates Δp, Δq, and Δr. In our numerical examples, these constraints have the following form:

$$\begin{aligned} -15 \le \Delta u \le 15, \\ -0.2618 \le \Delta\beta \le 0.2618, \\ -0.2618 \le \Delta p \le 0.2618, \\ -0.2618 \le \Delta q \le 0.2618, \\ -0.2618 \le \Delta r \le 0.2618 \end{aligned}$$

in which the angular rates Δp, Δq, and Δr are in radians per second, side slip angle $\Delta\beta$ is in radians, and the airspeed Δu is in meters per second.

The safety constraints are imposed on the airspeed $U = \Delta u + U_0$, the angle of attack $\alpha = \Delta\alpha + \alpha_0$, and the bank angle $\phi = \Delta\phi + \phi_0$ as follows:

$$\begin{aligned} U_{\min} \le \Delta u + U_0 \le U_{\max}, \\ \alpha_{\min} \le \Delta\alpha + \alpha_0 \le \alpha_{\max}, \\ -0.7854 \le \Delta\phi + \phi_0 \le 0.7854 \end{aligned}$$

In the preceding, $U_{\min}$, $U_{\max}$, $\alpha_{\min}$, and $\alpha_{\max}$ correspond to the boundaries of the flight envelope. In particular, $U_{\min}$ is selected as

$$U_{\min} = \max\{U_{\text{stall}}, U_{p,\min}\} \tag{63}$$

in which U_{stall} is calculated as

$$U_{\text{stall}} = \sqrt{\frac{2W}{\rho S C_{L,\max}\cos\phi_0}} \tag{64}$$

in which W is the weight of the aircraft, S is the surface area of the wings, ρ is the air density at the current altitude, and $C_{L,\max}$ is the maximum coefficient of lift. The value of $U_{P,\min}$ is the minimum real root of the following polynomial equation, which characterizes the relationship between the maximum power produced by the engine of a propeller-driven aircraft at a given altitude and the resulting airspeed:

$$\frac{1}{2}\rho S C_{D0} U_0^4 + W\sin(\gamma_0)U_0^2 - \eta P^s_{\max}\left(\frac{\rho}{\rho^s}\right)^m U_0 + \frac{2KW^2}{\rho S\cos^2\phi_0} = 0 \tag{65}$$

In the preceding, η is the propeller efficiency, P^s is the maximum engine power at sea level, ρ^s is the air density at sea level, C_{D0} is an air drag coefficient, K is the air friction constant, and all other parameters are previously defined. The value of $U_{\max}$ is calculated as maximum real solution to Eq. (65).

V. Numerical Examples

A. Recoverable Set Comparisons

In this section, we numerically construct and compare O_∞, R^I_∞, R^{ext}_∞, $R^{I,r}_\infty$, and $R^{\text{ext},I}_\infty$ for the trim condition corresponding to an airspeed of $U_0 = 60$ m/s, an altitude of 2500 m, a flight-path angle of $\gamma_0 = 0$ deg, and a bank angle of $\phi_0 = 0$ deg. The linearized models and the nominal longitudinal and lateral controllers have been given in Sec. IV.

For R^{ext}_∞ and $R^{\text{ext},I}_\infty$, a horizon of $H = 1$ was used to define the auxiliary subsystem. The value of $t^* = 15$ was used for all the sets (an upper bound). The time to calculate 121 different O_∞, O^I_∞, $O^{I,r}_\infty$, O^{ext}_∞, and $O^{\text{ext},I}_\infty$ sets (i.e., the time to form and stack up the inequalities in the polyhedral set representation) at 121 different trim points for linearized longitudinal and lateral dynamics (i.e., 1210 total sets, 605 for longitudinal dynamics, 605 for lateral dynamics) was recorded. The average time to calculate the sets O_∞, O^I_∞, and $O^{I,r}_\infty$ (726 total) was 0.0024 s per set without redundant constraint elimination and 1.7245 s per set with redundant constraint elimination. The average time to calculate the sets O^{ext}_∞ and $O^{\text{ext},I}_\infty$ (484 total) was 0.0036 s per set without redundant constraint elimination and 3.5155 s per set with redundant constraint elimination. These calculations were performed on a computer with 4 GB RAM running a 2.66 GHz duo-core processor using MATLAB 2012a. Fast calculation times of these sets indicate that their computation would be feasible onboard.

Figures 1 and 2 show projections of the safe and recoverable sets for the longitudinal linearized dynamics. Figures 3 and 4 show the projections of the safe and recoverable sets for the lateral linearized dynamics. Note that, in Fig. 1, R^I_∞, $R^{I,r}_\infty$, and $R^{\text{ext},I}_\infty$ are all the same size in this projection because they have reached the size of the initial constraints and hence overlap.

Based on the figures, O_∞ is the smallest compared with the other four sets, that is, $O_\infty \subset R^I_\infty$, $O_\infty \subset R^{\text{ext}}_\infty$, $O_\infty \subset R^{I,r}_\infty$, and $O_\infty \subset R^{\text{ext},I}_\infty$. These figures also confirm that $R^I_\infty \subset R^{I,r}_\infty$, $R^{\text{ext}}_\infty \subset R^{\text{ext},I}_\infty$, and $R^I_\infty \subset R^{\text{ext},I}_\infty$, which are facts that can be easily established theoretically. For the longitudinal dynamics (Figs. 1 and 2), it appears that the set inclusions $O_\infty \subset R^{\text{ext}}_\infty \subset R^I_\infty \subset R^{I,r}_\infty \subset R^{\text{ext},I}_\infty$ may hold, however, for the lateral dynamics (Figs. 3 and 4), $O_\infty \subset R^I_\infty \subset R^{I,r}_\infty \subset R^{\text{ext}}_\infty \subset R^{\text{ext},I}_\infty$. Note that, in general, the relative size relationships between R^I_∞ and R^{ext}_∞, $R^{I,r}_\infty$ and R^{ext}_∞, and $R^{I,r}_\infty$ and $R^{\text{ext},I}_\infty$ are problem dependent.

B. Connected Trim Points

We consider a set of destination trim points corresponding to $U_0 \in \{40, 45, 50, \ldots, 90\}$ m/s, $\gamma_0 \in \{-5, -4, \ldots, 5\}$ deg, $\phi_0 = 0$ deg, and an altitude of 2500 m. An initial trim point corresponds to an

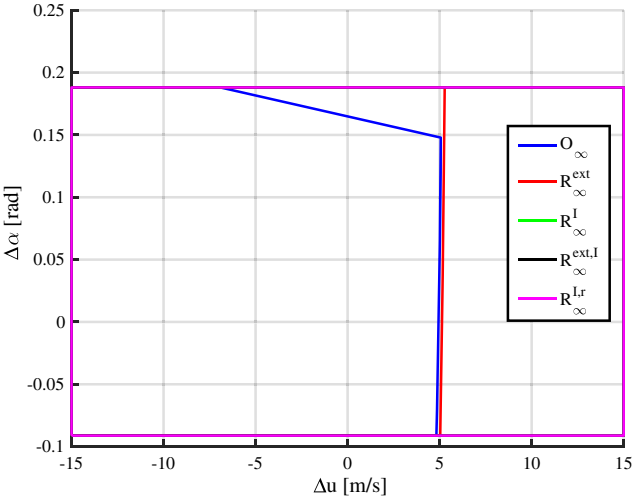

Fig. 1 Projections of the longitudinal O_∞, R^I_∞, R^{ext}_∞, $R^{I,r}_\infty$, and $R^{\text{ext},I}_\infty$ sets onto the $\Delta u - \Delta\alpha$ plane.

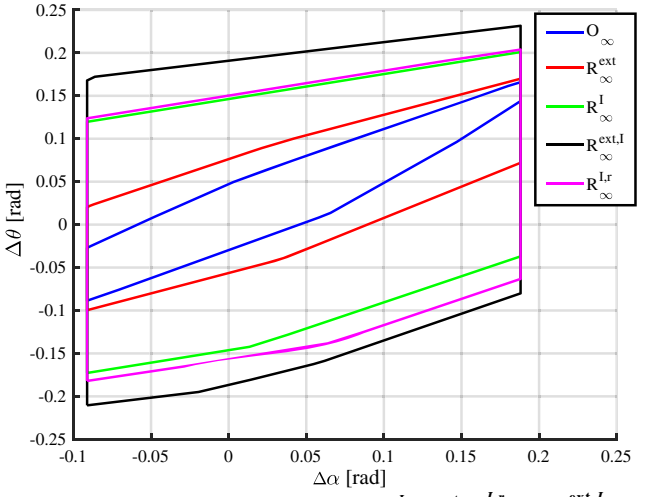

Fig. 2 Projections of the longitudinal O_∞, R^I_∞, R^{ext}_∞, $R^{I,r}_\infty$, and $R^{ext,I}_\infty$ sets onto the $\Delta\alpha - \Delta\theta$ plane.

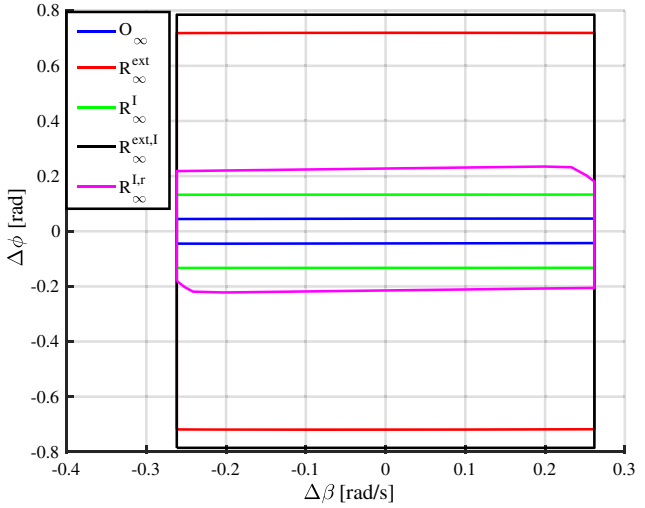

Fig. 3 Projections of the lateral O_∞, R^I_∞, R^{ext}_∞, $R^{I,r}_\infty$, and $R^{ext,I}_\infty$ sets onto the $\Delta\beta - \Delta\phi$ plane.

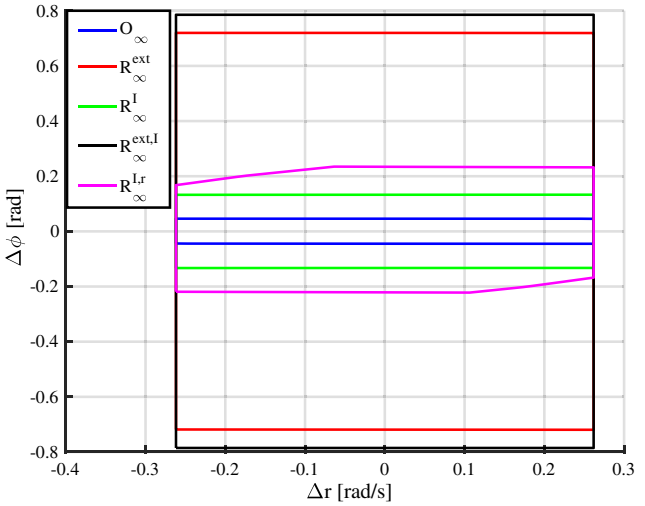

Fig. 4 Projections of the lateral O_∞, R^I_∞, R^{ext}_∞, $R^{I,r}_\infty$, and $R^{ext,I}_\infty$ sets onto the $\Delta r - \Delta\phi$ plane.

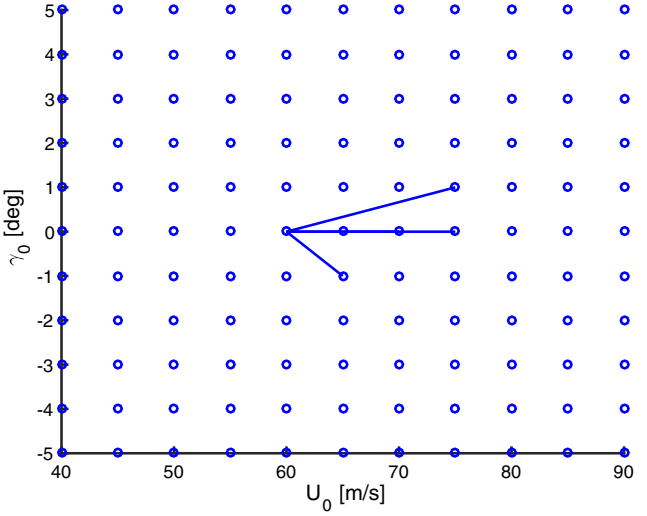

Fig. 5 Trim conditions (with $\phi = 0$ deg at an altitude of 2500 m) to which a safe transition from $U_0 = 60$ m/s and $\gamma_0 = 0$ deg using O_∞ is feasible. There are five connections total.

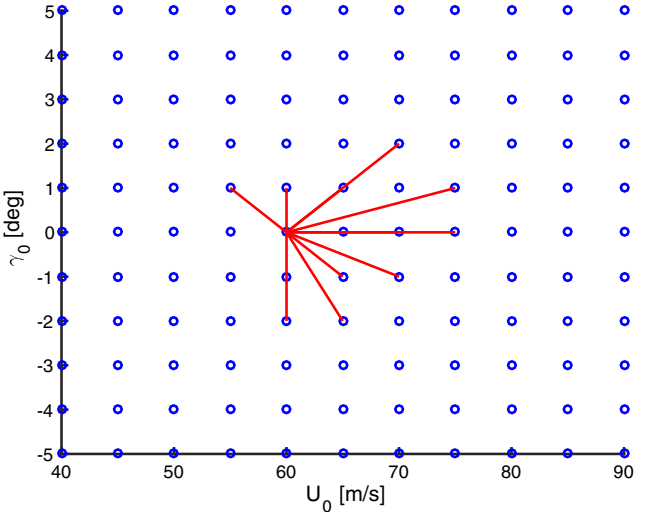

Fig. 6 Trim conditions (with $\phi = 0$ deg at an altitude of 2500 m) to which a safe transition from $U_0 = 60$ m/s and $\gamma_0 = 0$ deg using O^{ext}_∞ is feasible. There are 12 connections total.

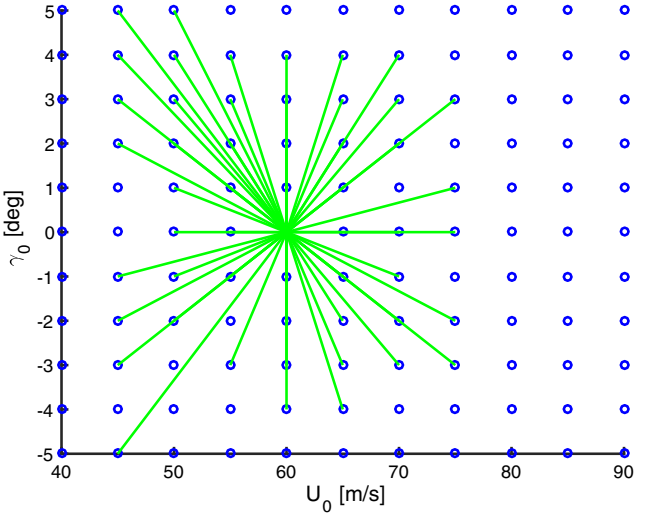

Fig. 7 Trim conditions (with $\phi = 0$ deg at an altitude of 2500 m) to which a safe transition from $U_0 = 60$ m/s and $\gamma_0 = 0$ deg using O^I_∞ is feasible. There are 51 connections total.

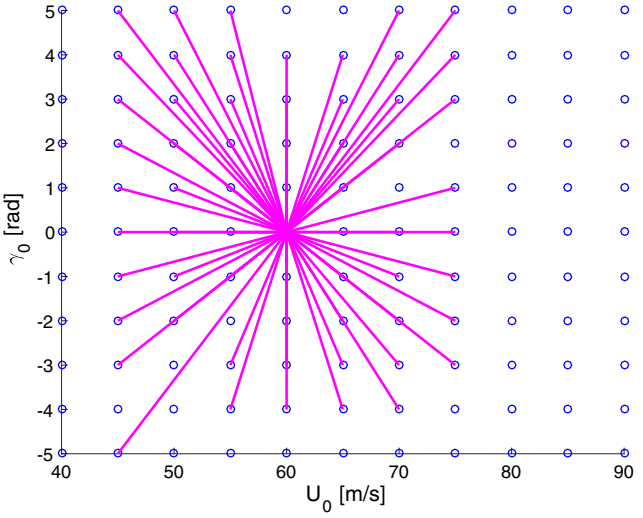

Fig. 8 Trim conditions (with $\phi = 0$ deg at an altitude of 2500 m) to which a safe transition from $U_0 = 60$ m/s and $\gamma_0 = 0$ deg using $O_\infty^{I,r}$ is feasible. There are 60 connections total.

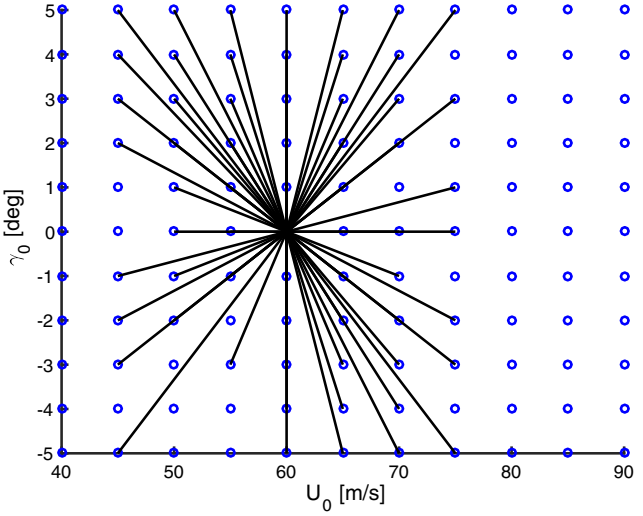

Fig. 9 Trim conditions (with $\phi = 0$ deg at an altitude of 2500 m) to which a safe transition from $U_0 = 60$ m/s and $\gamma_0 = 0$ deg using $O_\infty^{\text{ext},I}$ is feasible. There are 61 connections total.

airspeed of $U_0 = 60$ m/s, an altitude of 2500 m, a flight-path angle of $\gamma_0 = 0$ deg, and a bank angle of $\phi_0 = 0$. Based on the linearized models (52) and (57), the control schemes described earlier, and criteria (45–49), the set of trim conditions to which constrained admissible transitions from the initial trim point have been determined (see Figs. 5–9). In total, there are 120 possible transitions (not counting remaining at the starting trim condition).

Figure 5 shows the connections for O_∞. The use of O_∞ produces the fewest number of constraint-admissible connections: only five connections. Figure 6 shows the connections for O_∞^{ext}. The number of connections with O_∞^{ext} increases to 12. Figure 7 shows the connections for O_∞^{I}. There is a substantial increase in the number of constraint-admissible connections for O_∞^{I} as compared with O_∞^{ext}, with a total of 51 connections. Figure 8 shows the constraint-admissible connections for $O_\infty^{I,r}$, with 60 total connections. And finally, Fig. 9 shows the constraint-admissible connections for $O_\infty^{\text{ext},I}$, with a total of 61 connections.

C. Simulated Transitions Based on the Linearized Models

Transition trajectories from an initial trim point to a new trim point using different sets and respective control schemes are compared in Fig. 10, in which constraints are plotted as well. In the simulated transitions, the initial trim point corresponds to an airspeed of $U_0 = 60$ m/s, an altitude of 2500 m, a flight-path angle of $\gamma_0 = 0$ deg, and a bank angle of $\phi_0 = 0$ deg. The target trim condition corresponds to an airspeed of $U_0 = 75$ m/s, an altitude of 2500 m, a flight-path angle of $\gamma_0 = 1$ deg, and a bank angle of $\phi_0 = 0$ deg. Note that the transition trajectories based on O_∞ and O_∞^{ext} overlap one another. In the case of O_∞^{I}, we reset the integrator state according to Eq. (21) at discrete-time instants every $t_s = 0.1$ s. In the case of $O_\infty^{I,r}$, both the integrator state and the reference are reset according to Eq. (29) at discrete-time instants every $t_s = 0.1$ s. In the case of $O_\infty^{\text{ext},I}$, both the integrator state and the state of the auxiliary subsystem are reset according to Eq. (43) at discrete-time instants every $t_s = 0.1$ s.

The trajectories resulting from the use of O_∞^{I}, $O_\infty^{I,r}$, and $O_\infty^{\text{ext},I}$ and resets have substantially quicker convergence in the Δu state than the nominal trajectory without resets. Figure 11 shows the time histories of the two integral states of the controller and the Lyapunov function [which is used in Eq. (21)] for the trajectory in Fig. 10 that uses O_∞^{I}. Note that, in this case, the integrator state for the error in flight-path angle γ is kept artificially high until the integrator state for the error in airspeed has converged close to zero. The apparent chattering in the integrator state for γ is due to the integral state updates at discrete-time instants and its natural evolution in between the discrete-time instants.

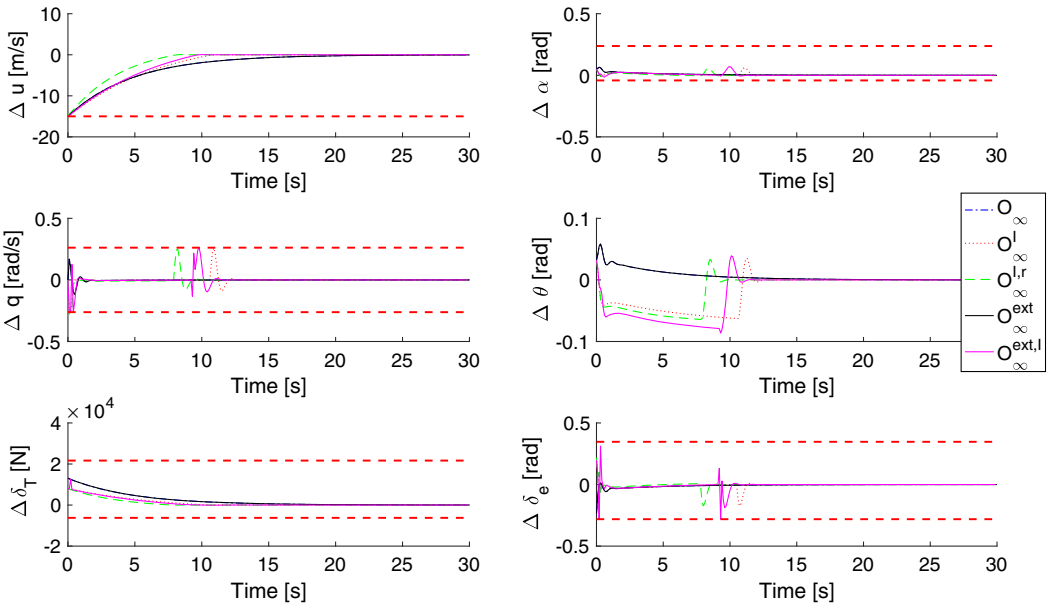

Fig. 10 Transition time histories from one trim point to another using different implementations. Constraints are shown by red dashed lines.

D. Nonlinear Model Simulations

Constraint-admissible trajectories developed based on the linearized model are now shown to remain constraint admissible or nearly constraint admissible based on the simulations on the nonlinear aircraft model [30]. The model's states are

$$X = [\,U \quad V \quad W \quad P \quad Q \quad R \quad \phi \quad \theta \quad \psi \quad \Theta_{\text{lat}} \quad \Theta_{\text{Long.}} \quad h_a\,]^T$$

in which U, V, and W are the body-fixed airspeeds; P, Q, and R are the body-fixed angular accelerations; ϕ, θ, and ψ are the body-fixed Euler angles; Θ_{lat} and $\Theta_{\text{Long.}}$ are latitude and longitude; and h_a is the altitude. The simulated control scheme is based on the use of $O_\infty^{I,r}$ sets and CSRG [17] to reset the integrator states and the reference command at discrete-time instants every $t_s = 0.1$ s according to Eq. (29).

Note the recursive feasibility of Eq. (29) is only guaranteed for the linearized model. If the feasibility is lost in the simulations on the nonlinear model, the integrator states are updated according to

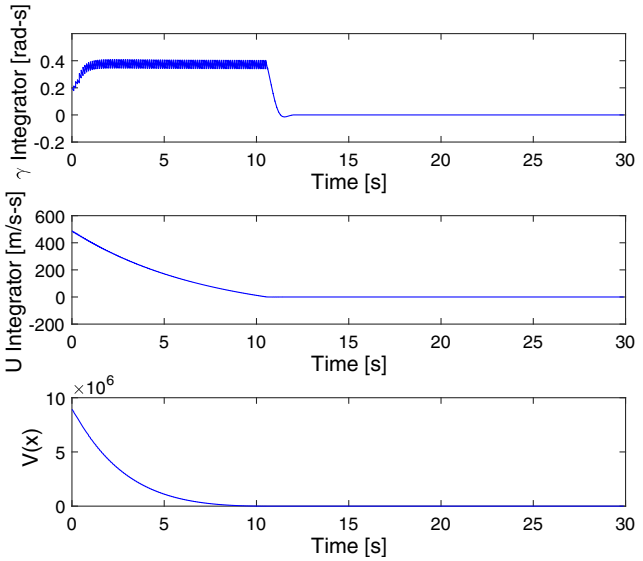

Fig. 11 Integrator states (top and middle plots) and Lyapunov function values (bottom plot) for trajectory from Fig. 10, corresponding to use of O_∞^I and controller state reset.

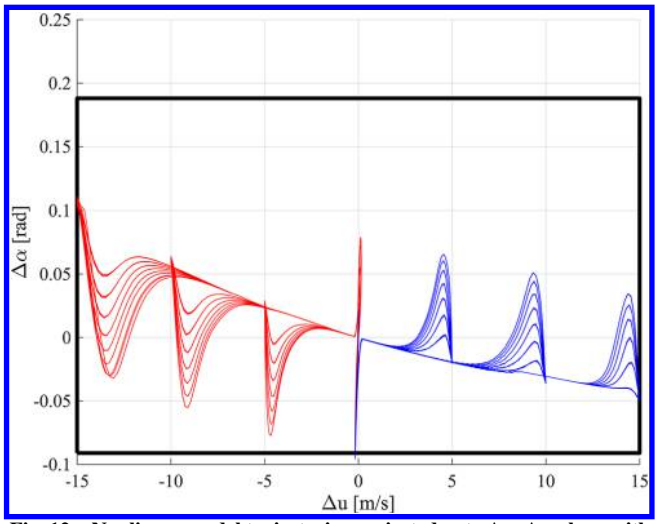

Fig. 12 Nonlinear model trajectories projected onto Δu–$\Delta\alpha$ plane with associated $R_\infty^{I,r}$. Note that red (lighter) trajectories satisfy constraints and blue (darker) ones slightly violate constraints (color in online).

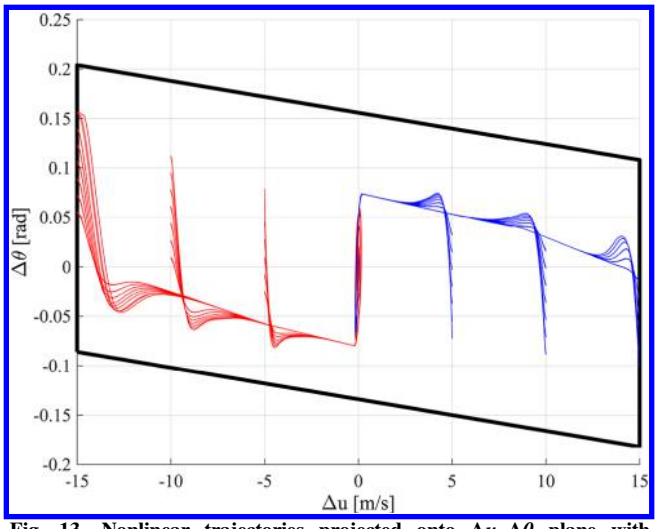

Fig. 13 Nonlinear trajectories projected onto Δu–$\Delta\theta$ plane with associated $R_\infty^{I,r}$. Note that blue (darker) trajectories in this figure represent those that violate the minimum α constraint as in Figs. 12 and 14.

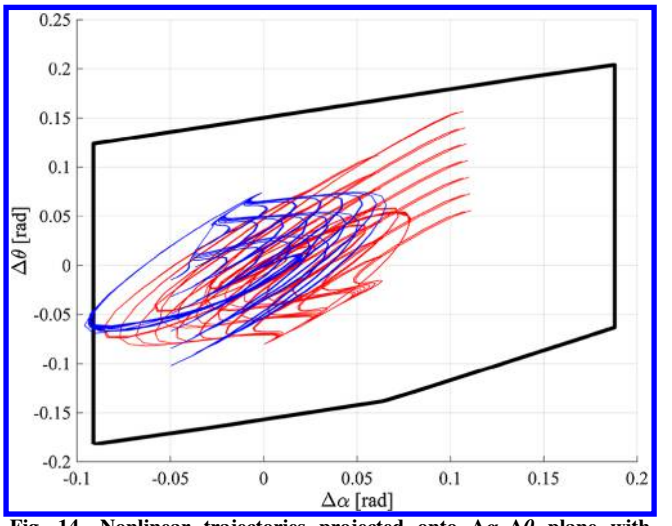

Fig. 14 Nonlinear trajectories projected onto $\Delta\alpha$–$\Delta\theta$ plane with associated $R_\infty^{I,r}$. Note that red (lighter) trajectories satisfy constraints and blue (darker) ones violate constraints (color in online).

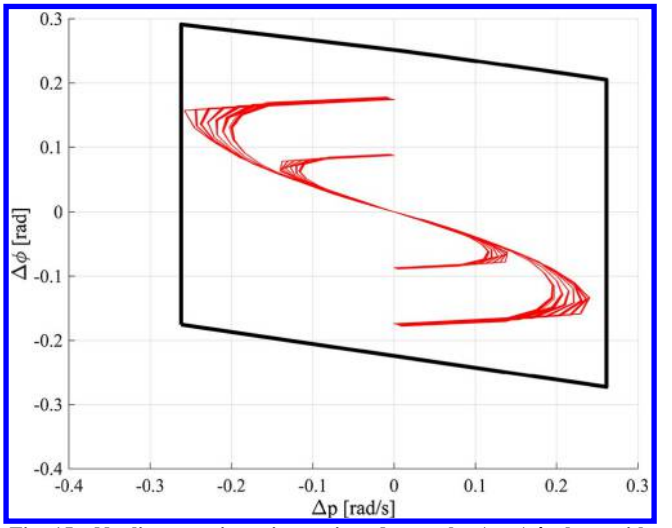

Fig. 15 Nonlinear trajectories projected onto the Δp–$\Delta\phi$ plane with associated $R_\infty^{I,r}$.

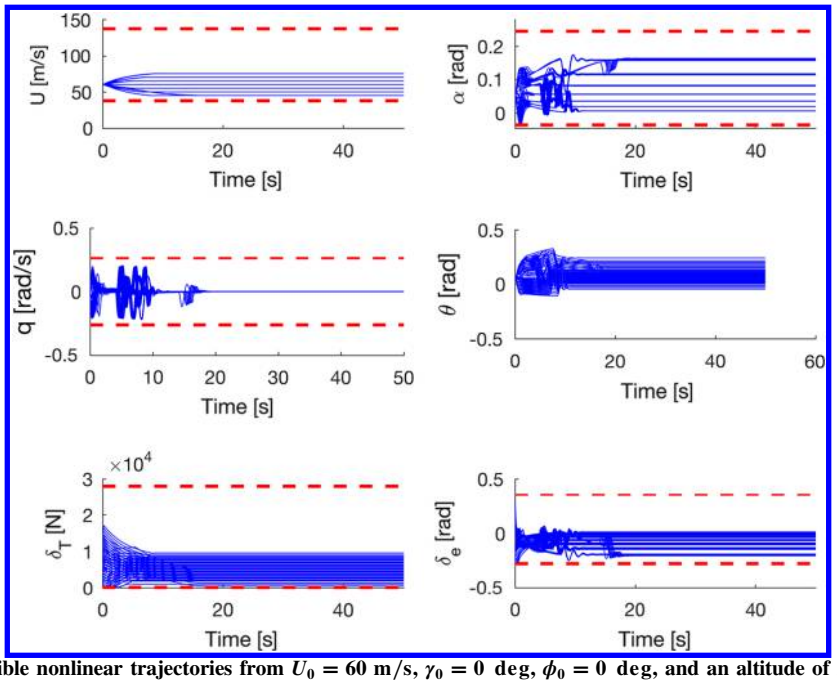

Fig. 16 Constraint-admissible nonlinear trajectories from $U_0 = 60$ m/s, $\gamma_0 = 0$ deg, $\phi_0 = 0$ deg, and an altitude of 2500 m to those that satisfy criterion (47).

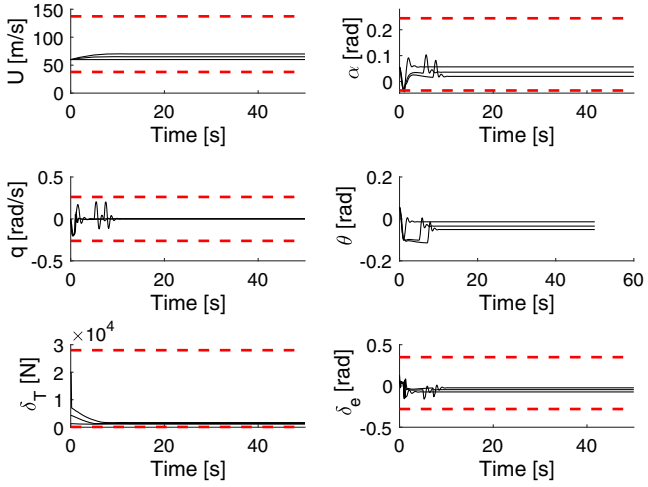

Fig. 17 Constraint violating nonlinear trajectories from $U_0 = 60$ m/s and $\gamma_0 = 0$ deg, $\phi_0 = 0$ deg, and an altitude of 2500 m to those that satisfy criterion (47).

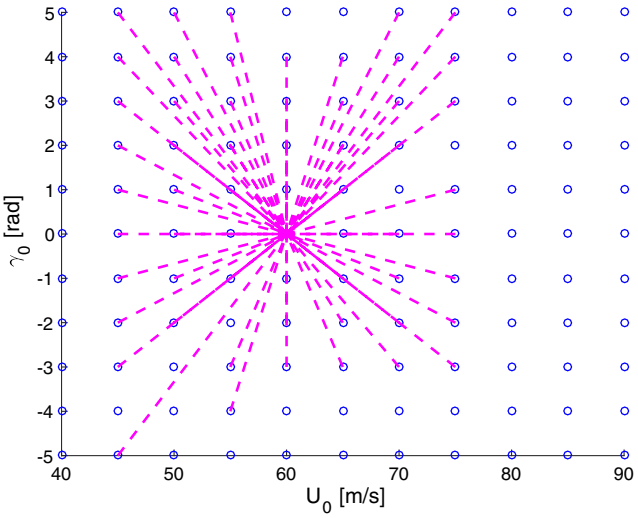

Fig. 18 Constraint-admissible connections from Fig. 8, maintained during nonlinear simulations. There are 57 connections total here (compared with 60 connections in the linear case).

their nominal dynamics and the reference is maintained at the previous value.

We first consider transitions to the target trim point corresponding to an airspeed of $U_0 = 60$ m/s, an altitude of 2500 m, a flight-path angle of $\gamma_0 = 0$ deg, and a bank angle of $\phi_0 = 0$ deg. The initial trim points were chosen from possible values of $U_0 \in \{30, 35, \ldots, 100\}$ m/s, $\gamma_0 \in \{-5, -4, \ldots, 5\}$ deg, $\phi_0 \in \{-30, -25, \ldots, 30\}$ deg, and altitude of 2500 m. The transitions from the initial trim points satisfying Eq. (47) were simulated using the nonlinear aircraft model. Figures 12–15 show the trajectories from trim conditions that satisfy Eq. (47) plotted over planar projections of $R^{I,r}_{\infty}$, corresponding to the target trim point. The red trajectories are constraint admissible in the projection and the blue trajectories violate constraints in the projection. The constraint being violated is the minimum α constraint. Its violation is very slight.

We next consider transitions from the same trim point to target trim points that are constraint admissible according to Eq. (47). The feasible transitions based on the linearized dynamics are identified in Fig. 8. Figures 16 and 17 show the results of these simulations, with

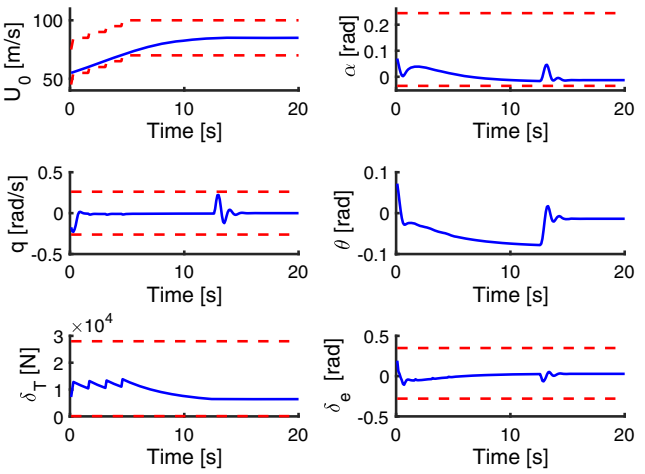

Fig. 19 Nonlinear state trajectories and control inputs when transitioning through a sequence of trim conditions. Note that no constraints (shown by dashed red lines) are violated due to use of CSRG control scheme and $O^{I,r}_{\infty}$ sets (color in online).

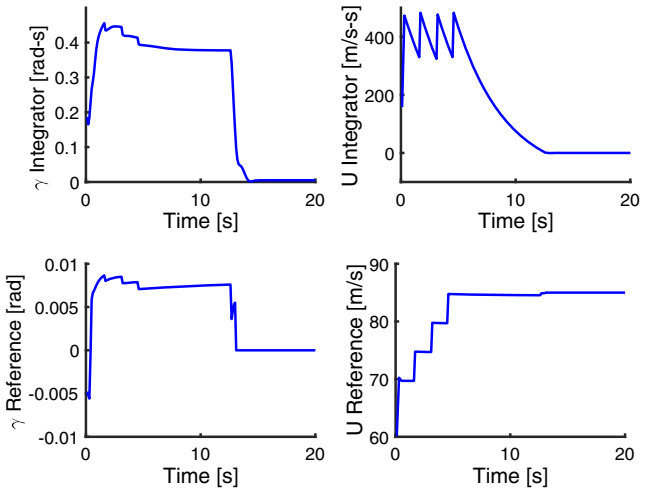

Fig. 20 Integrator states and reference signals when using CSRG control scheme and associated $O_{\infty}^{I,r}$ sets to transition through a sequence of trim conditions.

Fig. 18 showing which connections are constraint admissible (there are 57 total of the total 60). In Figs. 16 and 17, the relevant constraints are also shown, including the safety constraints (63) for U and α. The transitions to airspeeds of 60, 65, or 70 m/s and a flight-path angle of −4 deg result in trajectories that slightly (less than 0.01 rad) violate the minimum constraint on α.

Finally, we simulate transitions between a sequence of trim points satisfying Eq. (47) based on the linearized models. The initial trim point is at an airspeed of $U_0 = 55$ m/s, an altitude of 2500 m, a flight-path angle of $\gamma_0 = 0$ deg, and a bank angle of $\phi_0 = 0$ deg. The target trim point is at an airspeed of $U_0 = 85$ m/s, an altitude of 2500 m, a flight-path angle of $\gamma_0 = 0$ deg, and a bank angle of $\phi_0 = 0$ deg. The direct transition to the target trim point is not feasible [e.g., the change in airspeed violates the model validity constraints (63)]. However, by linking several "in-between" trim points together, a constraint-admissible trajectory can be obtained (see Figs. 19 and 20). In these simulations, a sequence of trim points X_{eq}^{i} is used that corresponds to the sequence of airspeeds $U_0 \in \{55, 60, 65, 70, 75, 80, 85\}$ m/s, all with an altitude of 2500 m, a flight-path angle of $\gamma_0 = 0$ deg, and a bank angle of $\phi_0 = 0$ deg. The feasibility of switching to the next set point in the sequence is checked every $t_s = 0.1$ s and occurs immediately once it is determined to be feasible based on Eq. (29), configured for the next trim point in the sequence; if not feasible yet, CSRG is still applied to reset the integrator states and reference commands based on Eq. (29), configured for the current trim point in the sequence.

Figure 19 shows the state trajectories and control sequences used plotted with the constraints used at each of the different trim conditions. Note that the only constraint that changes in time is the airspeed constraint. Figure 20 shows the integrator states and the references throughout this transition that are reset at discrete-time instants.

VI. Conclusions

The paper described several approaches to computing recoverable sets and recovery control sequences for use in aircraft LOC situations. The recoverable sets characterize the sets of initial conditions of the aircraft, for which there exists a recovery sequence generated through one of the recovery mechanisms that enables the aircraft to avoid constraint violation. The recovery mechanisms include resetting controller states, references, states of an auxiliary, finite-dimensional subsystem, and various combinations of the preceding. With these recovery mechanisms, the computations of the recoverable sets reduce to the computation of the conventional safe sets. If linear discrete-time models are used, these computations can be performed very rapidly and are feasible for onboard implementation. The simulations on the nonlinear aircraft model demonstrate that predictions of feasible trim-point-to-trim-point transitions between close-by trim points is fairly accurate based on linearized models. It has also been shown that the recoverable sets corresponding to different trim points can be chained together and transition logic can be defined to effect constraint-admissible transitions between trim points further apart.

Appendix: Aircraft Model

The aircraft model used in this paper is a model of the DHC-6 Twin Otter. This aircraft was chosen because it has a rich modeling history, which includes aerodynamic coefficient changes dues to wing icing [31]. The aerodynamic coefficients are from [29]. The nonlinear aircraft model is the standard model with the translational dynamics described by

$$\begin{aligned} m(\dot{U} - VR + WQ) &= -\sin(\theta)mg - \cos(\beta)\cos(\alpha)D + \sin(\alpha)L + \cos(\phi_T)F_T, \\ m(\dot{V} - UR + WP) &= \sin(\phi)\cos(\theta)mg - \sin(\beta)D, \\ m(\dot{W} - UQ + VP) &= \cos(\theta)\cos(\theta)mg - \cos(\beta)\sin(\alpha)D - \cos(\alpha)L - \sin(\phi_T)F_T \end{aligned} \tag{A1}$$

and the rotational dynamics described by

$$\begin{aligned} I_{xx}\dot{P} + (I_{zz} - I_{yy})QR - I_{xz}(\dot{R} + PQ) &= L_A + L_T, \\ I_{yy}\dot{Q} + (I_{xx} - I_{zz})PR - I_{xz}(P^2 - R^2) &= M_A + M_T, \\ I_{zz}\dot{R} + (I_{yy} - I_{xx})PQ - I_{xz}(QR - \dot{P}) &= N_A + N_T \end{aligned} \tag{A2}$$

A trim condition is defined as an equilibrium point of Eqs. (A1) and (A2). In the preceding, U, V, and W are the X, Y, and Z components of the airspeed, respectively; P, Q, and R are the angular speeds about the body-fixed X, Y, and Z axes, respectively; α is the angle of attack; θ is the pitch angle; ϕ is the bank angle; β is the sideslip angle; ϕ_T is the angle at which the thrust affects the aircraft; F_T is the thrust force; L_T, M_T, and N_T are the moments produced by the thrust; and the I terms are the aircraft moments of inertia. The aerodynamic forces are drag D and lift L. The aerodynamic moments are L_A, M_A, and N_A and are described by

$$\begin{aligned} D &= C_D p_d S, \\ L &= C_L p_d S, \\ L_A &= C_l p_d S b, \\ M_A &= C_m p_d S \bar{c}, \\ N_A &= C_n p_d S b \end{aligned} \tag{A3}$$

with $p_d = 1/2\rho U_0^2$ being the dynamic pressure and S, b, and $\bar{c}$ being aircraft-specific parameters. The aerodynamic coefficients C_D, C_L, C_l, C_m, and C_n, and the functions that describe them, for the DHC-6 Twin Otter are found in [29].

Equations (A1) and (A2) are linearized about a trim condition and algebraically manipulated to generate the following decoupled longitudinal and lateral linear dynamics models. The linearized longitudinal dynamics are described by

$$\begin{aligned}
\dot{\Delta u} &= \frac{-p_d S}{mU_0}(2C_{D0} + C_{Du})\Delta u + \frac{p_d S}{m}(C_{L0} + C_{D\alpha})\Delta\alpha + \frac{p_d Sc}{2\ mU_0}C_{Dq}\Delta q - g\Delta\theta + \frac{p_d S}{m}C_{D\delta_e}\delta_e + \frac{T_{\max}}{m}\delta_{th},\\
\dot{\Delta\alpha} &= \frac{-p_d S}{mU_0^2}(2C_{L0} + C_{Lu})\Delta u + \frac{-p_d S}{mU_0}(C_{L\alpha} + C_{D0})\Delta\alpha + (1 - \frac{p_d Sc}{2\ mU_0^2}C_{Lq})\Delta q - \frac{p_d S}{mU_0}C_{L\delta_e}\delta_e,\\
\dot{\Delta q} &= \frac{p_d SC}{I_{yy}U_0}(2C_{m0} + C_{mu})\Delta u + \frac{p_d Sc}{I_{yy}}C_{m\alpha}\Delta\alpha + \frac{p_d Sc^2}{2I_{yy}U_0}C_{mq}\Delta q - \frac{p_d Sc}{I_{yy}}C_{L\delta_e}\delta_e,\\
\dot{\Delta\theta} &= \Delta q
\end{aligned} \tag{A4}$$

and the linearized lateral dynamics are described by

$$\begin{aligned}
\dot{\Delta\beta} &= \frac{-p_d S}{mU_0}(C_{D0} + C_{E\beta})\Delta\beta + \frac{-p_d Sb}{2\ mU_0^2}C_{Ep}\Delta p + \left(\frac{p_d Sb}{2mU_0^2}C_{Er} - 1\right)\Delta r - \frac{p_d S}{mU0}C_{E\delta a}\delta a - \frac{p_d S}{mU0}C_{E\delta r}\delta r,\\
\dot{\Delta} p - \frac{I_{xz}}{I_{xx}}\dot{\Delta} r &= \frac{p_d Sb}{I_{xx}}C_{l\beta}\Delta\beta + \frac{p_d Sb^2}{2I_{xx}U_0}C_{lp}\Delta p + \frac{p_d Sb^2}{2I_{xx}U_0}C_{lr}\Delta r + \frac{p_d Sb}{I_{xx}}C_{l\delta a}\delta a + \frac{p_d Sb}{Ixx}C_{l\delta r}\delta r,\\
\dot{\Delta} r - \frac{I_{xz}}{I_{zz}}\dot{\Delta} p &= \frac{p_d Sb}{I_{zz}}C_{n\beta}\Delta\beta + \frac{p_d Sb^2}{2I_{zz}U_0}C_{np}\Delta p + \frac{p_d Sb^2}{2I_{zz}U_0}C_{nr}\Delta r + \frac{p_d Sb}{I_{zz}}C_{n\delta a}\delta a + \frac{p_d Sb}{Izz}C_{n\delta r}\delta r,\\
\dot{\Delta\phi} &= \Delta p
\end{aligned} \tag{A5}$$

In the preceding, there are several terms of the form C_{xy} which represent stability derivatives and derivatives of the force and moment coefficients (C_L, C_D, C_E, C_l, C_m, and C_n) with respect to the different states. Using C_{xy} as a template, x would be the force or moment (L, D, E, l, m, or n) and y would be the plant state (u, α, q, θ, β, p, r, ϕ). As an example, $C_{L\alpha}$ is the derivative of the coefficient of lift with respect to the angle of attack, that is, how the coefficient of lift changes as the angle of attack α changes.

There are several ways to calculate or estimate these stability derivatives, including wind-tunnel testing, computational fluid dynamics, or model identification. We used values from [29], which uses model identification techniques to fit polynomial expressions of plant states to known data of force and moment coefficients.

Acknowledgement

This research has been supported by the National Aeronautics and Space Administration under NASA Cooperative Agreement NNX12AM54A.

References

[1] Wilborn, J. E., and Foster, J. V., "Defining Commercial Transport Loss-of-Control: A Quantitative Approach," *AIAA Atmospheric Flight Mechanics Conference and Exhibit*, 2004, p. 4811.

[2] *Statistical Summary of Commercial Jet Airplane Accidents–Worldwide Operations 1959–2003*, Boeing Commercial Airplanes, Seattle, WA, 2004.

[3] Kwatny, H. G., Dongmo, J.-E. T., Chang, B.-C., Bajpai, G., Yasar, M., and Belcastro, C., "Aircraft Accident Prevention: Loss-of-Control Analysis," *AIAA Guidance, Navigation and Control Conference*, AIAA Paper 2009-6256, 2009.

[4] Kwatny, G., and Allen, R. C., "Safe Set Maneuverability of Impaired Aircraft," *Proceedings of AIAA Guidance Navigation and Control Conference and Exhibit*, AIAA, Reston, VA, 2012, pp. 12–16.

[5] Lygeros, J., "On Reachability and Minimum Cost Optimal Control," *Automatica*, Vol. 40, No. 6, 2004, pp. 917–927. doi:10.1016/j.automatica.2004.01.012

[6] Schuet, S., Acosta, D., Wheeler, K., Kaneshige, J., and Lombaerts, T., "An Adaptive Nonlinear Aircraft Maneuvering Envelope Estimation Approach for Online Applications," *AIAA Guidance, Navigation and Control Conference*, AIAA Paper 2014-0268, 2014.

[7] Bayen, A. M., Mitchell, I. M., Osihi, M. K., and Tomlin, C. J., "Aircraft Autolander Safety Analysis Through Optimal Control-Based Reach Set Computation," *Journal of Guidance, Control, and Dynamics*, Vol. 30, No. 1, 2007, pp. 68–77. doi:10.2514/1.21562

[8] Lombaerts, T., Schuet, S., Wheeler, K., Acosta, D., and Kaneshige, J., "Safe Maneuvering Envelope Estimation Based on a Physical Approach," *AIAA Guidance, Navigation, and Control Conference*, AIAA Paper 2013-4618, Aug. 2013.

[9] Pandita, R., Chakraborty, A., Seiler, P., and Balas, G., "Reachability and Region of Attraction Analysis Applied to GTM Dynamic Flight Envelope Assessment," *AIAA Guidance, Navigation, and Control Conference*, AIAA, Reston, VA, 2009, pp. 1–21.

[10] Tang, L., Roemer, M., Ge, J., Crassidis, A., Prasad, J., and Belcastro, C., "Methodologies for Adaptive Flight Envelope Estimation and Protection," *Proceedings of the Guidance, Navigation, and Control Conference*, AIAA Paper 2009-6260, 2009.

[11] Oort, E., Chu, Q., and Mulder, J., "Maneuver Envelope Determination Through Reachability Analysis," *Advances in Aerospace Guidance, Navigation and Control*, Springer, Berlin, 2011, pp. 91–102.

[12] Kolmanovsky, I., and Gilbert, E. G., "Multimode Regulators for Systems with State & Control Constraints and Disturbance Inputs," *Control Using Logic-Based Switching*, Springer, London, 1997, pp. 104–117.

[13] Weiss, A., Petersen, C., Baldwin, M., Erwin, R. S., and Kolmanovsky, I., "Safe Positively Invariant Sets for Spacecraft Obstacle Avoidance," *Journal of Guidance, Control, and Dynamics*, Vol. 38, No. 4, 2014, pp. 1–13.

[14] Blanchini, F., Pellegrino, F. A., and Visentini, L., "Control of Manipulators in a Constrained Workspace by Means of Linked Invariant Sets," *International Journal of Robust and Nonlinear Control*, Vol. 14, Nos. 13–14, 2004, pp. 1185–1205. doi:10.1002/(ISSN)1099-1239

[15] Kolmanovsky, I., and Sun, J., "A Multi-Mode Switching-Based Command Tracking in Network Controlled Systems with Pointwise-in-Time Constraints and Disturbance Inputs," *Sixth World Congress on Intelligent Control and Automation (WCICA 2006)*, Vol. 1, IEEE Publ., Piscataway, NJ, 2006, pp. 199–204.

[16] McDonough, K., Kolmanovsky, I., and Atkins, E., "Recoverable Sets of Initial Conditions and Their Use for Aircraft Flight Planning After a

Loss of Control Event," *AIAA Guidance, Navigation, and Control Conference*, AIAA Paper 2014-0786, 2014.

[17] McDonough, K., and Kolmanovsky, I., "Controller State and Reference Governors for Discrete-Time Linear Systems with Pointwise-in-Time State and Control Constraints," *American Control Conference (ACC)*, IEEE Publ., Piscataway, NJ, 2015, pp. 3607–3612.

[18] McDonough, K., and Kolmanovsky, I., "Integrator Resetting for Enforcing Constraints in Aircraft Flight Control Systems," *AIAA Guidance, Navigation, and Control Conference*, AIAA Paper 2015-1995, 2015.

[19] Gilbert, E. G., and Tan, K. T., "Linear Systems with State and Control Constraints: The Theory and Application of Maximal Output Admissible Sets," *IEEE Transactions on Automatic Control*, Vol. 36, No. 9, 1991, pp. 1008–1020. doi:10.1109/9.83532

[20] Kolmanovsky, I., and Gilbert, E. G., "Theory and Computation of Disturbance Invariant Sets for Discrete-Time Linear Systems," *Mathematical Problems in Engineering*, Vol. 4, No. 4, 1998, pp. 317–367. doi:10.1155/S1024123X98000866

[21] Gilbert, E. G., and Kolmanovsky, I. V., "Fast Reference Governors for Systems with State and Control Constraints and Disturbance Inputs," *International Journal of Robust and Nonlinear Control*, Vol. 9, No. 15, 1999, pp. 1117–1141.

[22] McDonough, K., "Developments in Stochastic Fuel Efficient Cruise Control and Constrained Control with Applications to Aircraft," Ph.D. Dissertation, Univ. of Michigan, Ann Arbor, MI, 2015.

[23] Aubin, J.-P., *Viability Theory*, Springer Science & Business Media, Berlin, 2009.

[24] Lombaerts, T., Schuet, S., Wheeler, K., Acosta, D., and Kaneshige, J., "Robust Maneuvering Envelope Estimation Based on Reachability Analysis in an Optimal Control Formulation," *2013 Conference on Control and Fault-Tolerant Systems (SysTol)*, IEEE Publ., Piscataway, NJ, 2013, pp. 318–323.

[25] Kalabic, U., Kolmanovsky, I., Buckland, J., and Gilbert, E., "Reference and Extended Command Governors for Control of Turbocharged Gasoline Engines Based on Linear Models," *IEEE International Conference on Control Applications (CCA)*, IEEE Publ., Piscataway, NJ, 2011, pp. 319–325.

[26] Rossiter, J. A., *Model-Based Predictive Control: A Practical Approach*, CRC Press, Boca Raton, FL, 2013.

[27] Yu, M.-J., McDonough, K., Bernstein, D. S., and Kolmanovsky, I., "Retrospective Cost Model Refinement for Aircraft Fault Signature Detection," *American Control Conference (ACC'2014)*, IEEE Publ., Piscataway, NJ, 2014, pp. 2486–2491.

[28] Coffer, B. C., Hoagg, J. B., and Bernstein, D. S., "Retrospective Cost Adaptive Control of the NASA GTM Model," *AIAA Guidance, Navigation, and Control Conference*, AIAA Paper 2010-8404, 2010.

[29] Grauer, J. A., and Morelli, E. A., "Generic Global Aerodynamic Model for Aircraft," *Journal of Aircraft*, Vol. 52, No. 1, 2014, pp. 13–20. doi:10.2514/1.C032888

[30] Stevens, B. L., and Lewis, F. L., *Aircraft Control and Simulation*, Wiley, Hoboken, NJ, 2003.

[31] Ranaudo, R. J., Mikkelsen, K. L., McKnight, R. C., and Perkins, P. J., "Performance Degradation of a Typical Twin Engine Commuter Type Aircraft in Measured Natural Icing Conditions," NASA Lewis Research Center, AIAA Paper 1984-0179, 1984.